THE INFLUENCE OF LARGE-SCALE ATMOSPHERIC CIRCULATION ON THE SURFACE ENERGY BALANCE OF THE KING GEORGE ISLAND ICE CAP

MATTHIAS BRAUN[a],*, HELMUT SAURER[a], STEFFEN VOGT[a], JEFFERSON CARDIA SIMÕES[b] and HERMANN GOßMANN[a]

[a] *Institut für Physische Geographie, Universität Freiburg, Werderring 4, D-79085 Freiburg, Germany*
[b] *Laboratório de Pesquisas Antárticas e Glaciológicas, Departamento de Geografia, Universidade Federal do Rio Grande do Sul, Av. Bento Gonçalves 9500, 91501-970 Porto Alegre, Brazil*

ABSTRACT

During the austral summer 1997–1998 three automatic weather stations were operated at different altitudes on the sub-Antarctic ice cap of King George Island (South Shetland Islands). Snowmelt was derived from energy balance computations. Turbulent heat fluxes were calculated from meteorological measurements using the bulk aerodynamic approach, with net radiation being measured directly. Modelled ablation rates were compared with readings at ablation stakes and continuously measured snow height at a reference site. Snow depletion and daily snowmelt cycles could be well reproduced by the model. Generally, radiation balance provided the major energy input for snowmelt at all altitudes, whereas sensible heat flux was a second heat source only in lower elevations. The average latent heat flux was negligible over the entire measuring period. A strong altitudinal gradient of available energy for snowmelt was observed. Sensible heat flux as well as latent heat flux decreased with altitude. The measurements showed a strong dependence of surface energy fluxes and ablation rates on large-scale atmospheric conditions. Synoptic weather situations were analysed based on AVHRR infrared quicklook composite images and surface pressure charts. Maximum melt rates of up to 20 mm per day were recorded during a northwesterly advection event with meridional air mass transport. During this northwesterly advection, the contribution of turbulent heat fluxes to the energy available for snowmelt exceeded that of the radiation balance. For easterly and southerly flows, continentally toned, cold dry air masses dominated surface energy balance terms and did not significantly contribute to ablation. The link between synoptic situations and ablation is especially valuable, as observed climatic changes along the Antarctic Peninsula are attributed to changes in the atmospheric circulation. Therefore, the combination of energy balance calculations and the analysis of synoptic-scale weather patterns could improve the prediction of ablation rates for climate change scenarios. Copyright © 2001 Royal Meteorological Society.

KEY WORDS: ablation; Antarctica; climatic change; King George Island; snowmelt; South Shetland Islands; surface energy balance; synoptic climatology

1. INTRODUCTION

Large-scale weather systems are the main cause of energy exchange in the atmosphere between the mid and high latitudes. Air masses of different origins are transported over ocean or land surfaces, resulting in variable air temperature and humidity. Therefore, energy fluxes near the surface are strongly influenced by synoptic conditions. Neal and Fitzharris (1997) have pointed out that little is known about the interrelationship between large-scale atmospheric processes on the one hand, and energy exchange between atmosphere and snow and ice surfaces on the other. This knowledge, however, is a prerequisite for the downscaling and validation of general circulation models (GCMs), as well as for the estimation and prediction of possible consequences of climatic change.

---

* Correspondence to: Institut für Physische Geographie, Universität Freiburg, Werderring 4, D-79085 Freiburg, Germany; e-mail: mabra@ipg.uni-freiburg.de

Climatic conditions along the Antarctic Peninsula differ greatly from the main Antarctic continent. Due to its location as a major obstacle in the circumpolar westerlies of the Southern Hemisphere, the Antarctic Peninsula experiences a pronounced latitudinal and longitudinal climatic differentiation (Reynolds, 1981; Braun and Schneider, 2000). An extraordinary high warming trend during the last decades was reported for several permanent stations along the Antarctic Peninsula (e.g. King, 1994; Stark, 1994; Harangozo *et al.*, 1997; Skvarca *et al.*, 1998). However, for the South Shetland Islands, the interannual variability of monthly mean air temperature and the warming trend are smallest. A link between air temperature, sea ice coverage and the Southern Oscillation Index (SOI) was reported by King (1994) and Smith *et al.* (1996). King and Harangozo (1998) investigated possible driving mechanisms for the temperature increase. They concluded that the circulation over the Antarctic Peninsula is now more northerly in winter than it was in the 1950s and 1960s. Similar indications were given by Turner *et al.* (1997), who investigated long-term precipitation records from Faraday and Rothera. They attributed the increase in the number of precipitation events to a greater number of depressions approaching from outside the Antarctic rather than from the west.

Although glaciological and meteorological studies of Antarctica have increased, little is known about the actual state and sensitivity of the ice masses to climatic changes. Few studies have attempted to calculate or measure energy fluxes at the snow surface in these latitudes (Braun and Schneider, 2000). From surface energy balance calculations on Ecology Glacier on King George Island (Figure 1), Bintanja (1995) suggested that an increase of air temperature by 1 K would result in a rise in ablation rates of about 15%. Furthermore, a sensitivity study using an ice flow model revealed a high sensitivity of the ice cap of King George Island to climatic changes (Knap *et al.*, 1996). According to this study, the Intergovernmental Panel of Climate Change (IPCC-90) 'business-as-usual' scenario with 1 K temperature increase would result in a drastic decrease of ice volume by about 36%. It was also predicted that the retreat of the ice margins would be higher on the southern than on the northern coast. In fact, the studies by Wunderle (1996), Park *et al.* (1998) and Simões *et al.* (1999) detected an impressive glacier retreat on
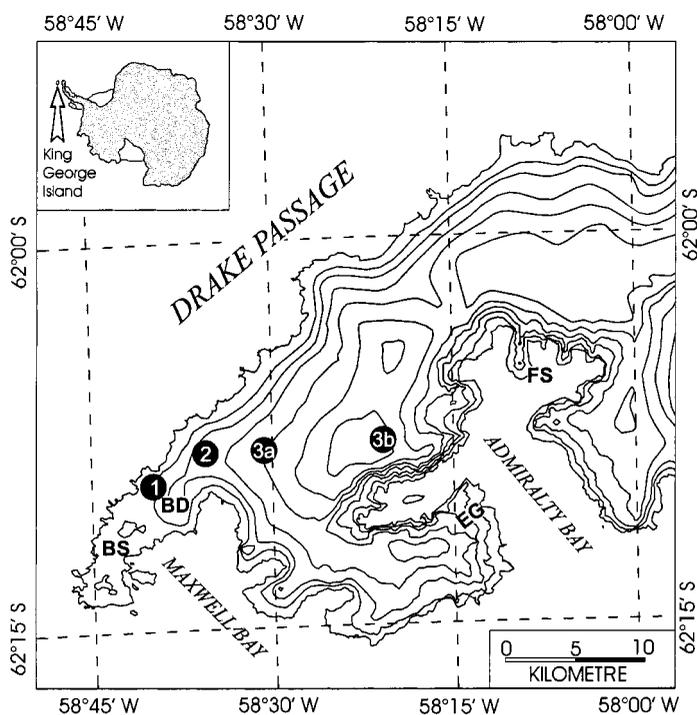
Figure 1. Map of western part of King George Island showing contour lines at 100 m intervals. The locations of the AWS are indicated by numbers. BS, Bellingshausen Station; BD, Bellingshausen Dome; EG, Ecology Glacier; FS, Ferraz Station

King George Island since 1956. Braun *et al.* (2000) showed indications for an increase in equilibrium line altitude since the mid-1970s. In contrast, Wen *et al.* (1994, 1998) concluded from mass balance studies on the Collins or Bellingshausen Dome, that this small ice cap was in steady state between 1971 and 1991. These conflicting results suggest that more research on glacier mass balance terms of the King George Island ice cap is essential for the prediction of the ice cap's behaviour during climatic changes.

The objective of this work is to determine the contribution of the individual energy balance terms to ablation and to demonstrate their dependence on large-scale atmospheric circulation patterns. In this context, the selected study area at King George Island is considered representative for ice caps on the South Shetland Islands.

2. STUDY AREA

With about 1250 km², 93% being ice covered, King George Island is the largest island of the South Shetland Islands. In the study area, the ice cap extends up to 679 m above sea level (a.s.l.) and is characterized by smooth slopes on the northern side and steep slopes and large outlet glaciers on the southern and eastern parts of the ice cap.

The location of the ice cap at the northern tip of the Antarctic Peninsula results in a climate predominated by the frequent succession of eastward moving low pressure centres (Jones and Simmonds, 1993; Turner and Leonard, 1996). This fact and its location near the edge of sea ice coverage during winter leads to a relatively warm, maritime climate. The low annual variability of mean monthly air temperatures (Figure 2), as reported by Smith *et al.* (1996), is a result of the location of the island in the circumpolar westerly wind zone of the Southern Hemisphere. Occasional barrier winds along the east coast of the Antarctic Peninsula advect cold dry air masses towards the South Shetland Islands (Schwerdtfeger, 1984; Parish, 1989). During the summer months, air temperature at sea level rises well above 0°C. Strong snowmelt events may also occur during the winter, as reported by Rachlewicz (1997). Owing to the occurrence of Föhn-type winds and decreased cloud amount, the average annual air temperature in Admiralty Bay is a few tenths of a degree higher than on the northwestern side (Martianov and Rakusa-Suszczewski, 1990). Strong altitudinal gradients of annual precipitation were reported, starting with approximately 500 mm at sea level (Bellingshausen station) and reaching more than 2000 mm in the highest parts of the ice cap (Wen *et al.*, 1998).

3. DATABASE

From 2 December 1997 to 12 January 1998, three automatic weather stations (AWS) were operated along an altitudinal profile (85, 255 and 385/619 m a.s.l.) on the King George Island ice cap. The AWS locations
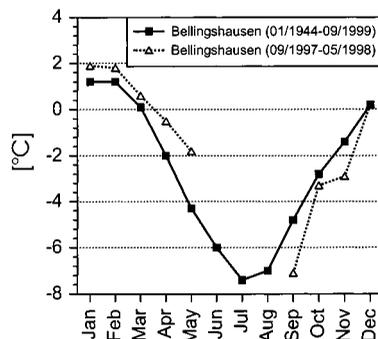
Figure 2. Monthly mean air temperature (January 1944–September 1999) at Bellingshausen Station, King George Island (solid line). The monthly mean air temperature for the period September 1997–May 1998 is indicated by the dashed line

are marked in Figure 1. AWS 3 was moved on 17 December 1997 from 385 m a.s.l. to 619 m a.s.l, as weather conditions proved to be better than expected and hoarfrost on the sensors rarely occurred, even at altitudes greater than 400 m a.s.l. The location of site 3B, close to an advanced camp, enabled shorter maintenance intervals of the AWS. All AWSs were instrumented at two levels (0.5 and 2.0 m) with Vaisala HMP35 air temperature and relative humidity sensors as well as with cup anemometers for the measurement of wind speed. Radiation and Energy Systems Q7 net radiometers provided direct radiation balance data. Albedo was calculated from readings of two SKYE SP1110 pyranometers at each AWS site. Additionally, the lowermost AWS was equipped with a continuously recording Campbell SR50 snow depth sensor and a tipping bucket rain gauge. The ablation stakes and the tripod of the SR50 sensor were drilled into the ice. All measurements were performed over snow. The sensors were sampled every 10 s, and data were recorded as 10-min and as hourly averages. All instruments were carefully calibrated before and after the field campaign. All AWSs were maintained in 2–7 day intervals. Snow depletion was measured at ablation stakes near the AWS sites, while snow density data were collected at nearby snow pits. It was observed that snow density only varied between 480 and 510 kg m^{-3}. Therefore, a mean density value of 500 kg m^{-3} was used in the derivation of snow water equivalent (WE). Hourly readings of surface air pressure data from the adjacent Brazilian station Commandante Ferraz were used for further computations and data analyses.

Surface pressure charts and National Ocean and Atmosphere Administration (NOAA) Advanced Very High Resolution Radiometer (AVHRR) infrared (IR) quicklook composites provided by the University of Wisconsin were available every 12 h during the entire observation period. Additional information about upper-air masses was obtained from daily radio soundings at Bellingshausen station.

4. METHODOLOGY

4.1. *Energy balance model*

In the following, the term 'ablation' refers to surface ablation only. Refreeze of meltwater in deeper snow layers is not considered in this investigation; the usage of the term 'ablation' therefore differs from the expression used in glaciological mass balance calculations.

The surface energy balance of a melting snow cover is given by

$$Q_M = Q_N + Q_H + Q_E + Q_G + Q_R \tag{1}$$

where Q_M is the energy available for melt, Q_N is the net radiation, Q_H is the sensible heat transfer, Q_E is the latent heat flux, Q_G is the ground heat flux and Q_R is the heat supplied by rain. Energy fluxes towards the surface are regarded as positive and those from the surface as negative. Ground heat flux was neglected since temperature profiles in the snow pits revealed a 0°C isotherm snow cover in the uppermost 2 m. Likewise, a previous study by Bintanja (1995) reported a very low conductive heat flux for King George Island, since surface temperatures were nearly constant at 0°C. Heat supplied by rain was calculated following the approach of Braun (1985). Since net radiation was measured directly, only the turbulent heat fluxes had to be computed from the hourly meteorological data. Therefore, a bulk aerodynamic approach model (Schneider, 1999a) was performed to compute latent and sensible heat flux, following the equations given by Oke (1970) and Moore (1983). This is discussed in more detail by Braithwaite (1995) and Blackadar (1997). When the air temperature was above 0°C, values from both the lower measuring level and the surface were used to ensure that all calculations were performed within the surface boundary layer. This assumed that the snow surface temperature was 0°C and postulated the occurrence of saturation conditions with respect to ice

$$Q_H = \frac{\rho c_p \kappa^2 u(z_1)}{\left[\ln\left(\frac{z_1}{z_{0,u}}\right) \ln\left(\frac{z_1}{z_{0,T}}\right) \right]} (\Theta(z_1) - \Theta_0)(1 - 5Rb)^2 \tag{2}$$

$$Q_L = \frac{\rho L_v 0.622 \kappa^2 u(z_1)}{p \left[\ln\left(\frac{z_1}{z_{0,u}}\right) \ln\left(\frac{z_1}{z_{0,q}}\right) \right]} (e(z_1) - e_0)(1 - 5Rb)^2 \tag{3}$$

In the case of negative temperatures, turbulent fluxes were calculated from the gradients between the two measuring levels. This led to the following formulas:

$$Q_H = \frac{\rho c_p \kappa^2 (u(z_2) - u(z_1))}{\left[\ln\left(\frac{z_2}{z_1}\right) \right]^2} (\Theta(z_2) - \Theta(z_1))(1 - 5Rb')^2 \tag{4}$$

$$Q_L = \frac{\rho L_v 0.622 \kappa^2 (u(z_2) - u(z_1))}{p \left[\ln\left(\frac{z_2}{z_1}\right) \right]^2} (e(z_2) - e(z_1))(1 - 5Rb')^2 \tag{5}$$

The variables are ρ, density of air; c_p, specific heat at constant pressure of air (1005 J kg^{-1} K^{-1}); κ, van Karman's constant (0.4); L_v, latent heat of evaporation/sublimation [(2.514/2.849) 10^6 J kg^{-1}]; p, air pressure; z_1, z_2, height above snow surface (0.5 m, 2.0 m); $u(z_1), u(z_2)$, wind velocity at height z_1, z_2; $z_{0,u}, z_{0,T}, z_{0,q}$, roughness lengths for momentum, heat and water vapour; $\Theta(z_1), \Theta(z_2)$, potential temperature at height z_1, z_2; Θ_0, potential temperature at the snow surface (0°C); $e(z_1), e(z_2)$, water vapour pressure at height z_1, z_2; e_0, water vapour pressure at the snow surface (6.1 hPa); Rb, Rb', bulk Richardson number, $Rb, Rb' < 0.2$; g, acceleration due to gravity.

Correction for stable stratification was performed using the bulk Richardson number. The correction terms were applied only for $Rb < 0.2$. In case of stable conditions ($Rb \geq 0.2$), the turbulent fluxes would be forced to zero. However, such conditions occurred in less than 5% of all measurements. The bulk Richardson number was calculated as follows:

$$Rb = \frac{g(\Theta(z_1) - \Theta_0)(z_1 - z_0)}{\frac{\Theta(z_1) + \Theta_0}{2} u(z_1)^2} \tag{6}$$

$$Rb' = \frac{g(\Theta(z_2) - \Theta(z_1))(z_2 - z_1)}{\frac{\Theta(z_2) + \Theta(z_1)}{2} (u(z_2) - u(z_1))^2}$$

Surface roughness lengths were used as tuning parameters, since no direct measurements of this parameter were available. All roughness lengths were assumed to be equal ($z_0 = z_{0u} = z_{0t} = z_{0e}$), which results in the effective roughness length as proposed by Morris and Harding (1991) and Braithwaite (1995). A z_0 value of 5.0×10^{-4} was used for the AWS site 1, whereas a value of $z_0 = 1.0 \times 10^{-3}$ was used for the remaining sites. These roughness lengths over snow are well documented in previous studies (e.g. Kuhn, 1979; Moore, 1983; Morris, 1989; Hock, 1998).

Model performance was validated by comparing modelled snow depletion against the measured ablation at AWS sites 1 and 2, as well as against the continuous snow height record obtained from the SR50 sensor at AWS site 1. For AWS site 3b (619 m a.s.l.), located near the highest point of the ice cap, no concurrent ablation record was available. Therefore, the respective z_0 values of AWS site 2 and the former AWS site 3a (385 m a.s.l.) were used. An evaluation of a 10-m snow temperature profile suggested that refreeze conditions are likely to occur in deeper layers of the snow cover at maximum altitudes. Hence, not all meltwater resulting from the available energy input would be transformed into discharge at this elevation.

Owing to insufficient power supply, radiation shields of the temperature and humidity probes could not be ventilated. This may result in biased measurements due to radiative heating. However, mean wind speed on the ice cap was well over 4 m s^{-1} (Table I), and periods of low wind speed rarely occurred. Errors resulting from insufficient ventilation of the temperature and humidity readings were therefore expected to be small and deemed negligible. This conclusion is supported by an error estimation given by Schneider (1999b). He used a similar data set for energy balance calculations at a test site further to the

south in Marguerite Bay. A detailed study on the accuracy of HMP35 humidity probes at temperatures below the freezing point was done by Anderson (1994).

4.2. Analysis of synoptic situations

While numerous studies have focussed on the high variability of depression tracks near the Antarctic Peninsula (e.g. Jones and Simmonds, 1993; Turner *et al.*, 1998), typical circulation patterns have received little attention. Based on surface pressure charts, Kejna (1993) classified the atmospheric circulation types in the region of the South Shetland Islands. As a result, 21 typical synoptic situations were identified for the period 1986–1989. Unfortunately, the classification methodology was not described in detail, thus an application to the current data set was not possible.

Four typical synoptic circulation patterns dominating extensive time periods were therefore extracted from the data. They were classified according to the subjective criteria of direction of air mass advection. The location of pressure centres and resulting direction of air mass transport were derived from 12-h AVHRR IR-composites, surface pressure charts with a similar time resolution and the prevailing wind direction at the AWS sites. A verification of the classification was done using the daily radio sounding data available from Bellingshausen station. Mesocyclones were not included in the analysis, since their average life time (< 12 h) is shorter than the temporal resolution of the available composite data (Heinemann, 1995; King and Turner, 1997).

The classified synoptic circulation patterns are now listed in the chronological order of their occurrence during the observation period:

 (a) advection from north to northwest
 (b) southerly to southeasterly air mass transport
 (c) advection from northwest
 (d) advection from west to southwest

5. RESULTS

5.1. Surface energy balance and ablation

Over the entire measuring period the calculated snowmelt agrees well with the measured water equivalent decrease. The correlation between measured and modelled snow depletion at AWS 1 is shown

Table I. Mean values of meteorological variables and surface energy balance components at the different AWS sites (2 December 1997–12 January 1998)

Parameter	AWS 1	AWS 2	AWS 3a	AWS 3b
Altitude (m a.s.l.)	85	255	385	619
Measuring period	2 Dec 1997– 12 Jan 1998	2 Dec 1997– 12 Jan 1998	6 Dec 1997– 17 Dec 1997	19 Dec 1997– 11 Jan 1998
Air temperature at 2 m (°C)	−0.03	−0.95	−0.63	−3.83
Relative humidity at 2 m (%)	92.1	93.1	97.5	97.6
Wind speed at 2 m (m s^{-1})	4.9	5.25	3.84	6.0
Downward short-wave radiation (W m^{-2})	214.5	248.5	253.9	287.6
Upward short-wave radiation (W m^{-2})	176.7	204.4	205.9	248.9
Albedo (%)	82.3	82.3	81.1	86.5
Net radiation (W m^{-2})	22.5	19.9	16.4	3.0
Sensible heat flux (W m^{-2})	9.5	1.5	−3.0	−2.4
Latent heat flux (W m^{-2})	−1.1	−3.1	−2.3	−3.2
Sum of energy balance components (W m^{-2})	31.0	18.4	11.1	−2.7

in Figure 3. Correlation coefficients ($r^2 = 0.99$) for both validations, modelled ablation against ablation sticks and modelled ablation against the snow depth sensor, are extraordinarily high. Even the marked daily cycle in snowmelt as observed with the continuous snow depth sensor could be reproduced in the model run. For the AWS 2 site, similar agreements between modelled and measured ablation were achieved ($r^2 = 0.99$). In the following we refer mainly to AWS 1, since this AWS provided a continuous data record throughout the field campaign. Over the 42 days of measurement, the model underestimated snowmelt at AWS 1 by 3% (383 mm WE compared with a measured WE decrease of 394 mm). This ablation rate equalized the encountered winter accumulation at the test site. Continuous ice melt occurred until March 1998.

It should be noted that the observed model performance resulted from adjustments via the roughness lengths and that the accuracy of temperature and humidity readings are influenced by unventilated radiation shields. Therefore, a sensitivity analysis (Table II) was performed to estimate the error due to these factors. Table II shows that the adjustment of roughness lengths is crucial for the magnitude of the calculated turbulent fluxes. However, keeping this parameter to values reported over snow and ice, the general partitioning of the energy balance components remains. Inaccuracies in the temperature measurements mainly influence the sensible heat flux, whereas latent heat flux is less sensitive to changes of this variable. The addition of 1 K to measured values is often used to simulate climate change conditions. The calculations show that sensible heat flux and ablation would increase drastically. However, it should be considered that the alteration of only one variable would not reflect real conditions, e.g. changes in radiation balance and wind conditions are not taken into account. Changes in relative humidity cause only very small variations in the distribution of energy fluxes, since the mean latent heat flux over the observation period is almost negligible. The increase of humidity values especially shows low influence. This can be attributed to the fact that measured relative humidity values are frequently close to saturation conditions. The results of this sensitivity analysis permit us to deduce at least some general characteristics of energy balance components on the King George Island ice cap from the model runs.

Figure 4 shows the development of individual energy balance terms, of the resulting sum of energy balance components, of calculated hourly melt rates and of snow depletion throughout the measuring period. The results obtained from snow depletion observations allowed the division of the entire research period into three major ablation phases:

1. from the beginning of the measurements until mid-December, a phase of relatively strong ablation took place. Temperatures were well above the freezing point and high relative humidity values indicate air mass transport over the ice-free Bellingshausen Sea and Drake Passage. This phase was followed by
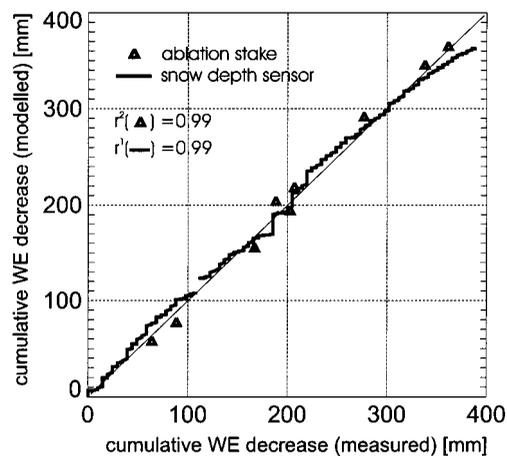
Figure 3. Correlation between measured and modelled WE decrease

Table II. Sensitivity analysis of energy balance calculations at AWS 1 (85 m a.s.l.)

Varied parameter/ variable	Sum of energy balance components (W m^{-2})	Latent heat flux (W m^{-2})	Sensible heat flux (W m^{-2})	Modelled ablation (mm)
$z_e = 1 \times 10^{-5}$	25.3	−1.8	4.5	309.3
$z_e = 1 \times 10^{-4}$	27.8	−1.6	6.8	340.4
$z_e = 5 \times 10^{-4}$	**31.0**	**−1.1**	**9.5**	**383.2**
$z_e = 1 \times 10^{-3}$	33.9	−0.7	12.0	412.7
$z_e = 1 \times 10^{-2}$	54.5	4.0	27.9	646.9
AT−1.0 K	23.0	−2.7	3.1	301.0
AT−0.3 K	28.8	−1.2	7.4	356.8
AT−0.1 K	30.6	−1.1	9.1	374.2
AT ± 0.0 K	**31.0**	**−1.1**	**9.5**	**383.2**
AT+0.1 K	32.3	−1.2	10.9	393.2
AT+0.3 K	33.6	−1.6	12.6	410.8
AT+1.0 K	41.0	−2.6	20.9	482.7
RH−5%	28.2	−3.9	9.5	363.4
RH−3%	29.4	−2.7	9.5	372.6
RH−1%	30.4	−1.6	9.5	380.0
RH ± 0%	**31.0**	**−1.1**	**9.5**	**383.2**
RH+1%	31.3	−0.7	9.5	386.1
RH+3%	32.0	0.0	9.5	391.0
RH+5%	32.7	0.7	9.5	394.9

Mean values for the period 2 December 1997–12 January 1998.
z_e denotes the varied effective roughness length, AT for air temperature and RH for relative humidity. The mean value of the radiation balance (22.5 W m^{-2}) was not altered in any of the sensitivity runs.

2. a period with almost no snowmelt with temperatures below 0°C until the end of the year. During this time, cold dry air masses, originating from the Antarctic continent, dominated the surface energy fluxes over the snow cover on the King George Island ice cap.
3. With New Year's Eve 1997, phase 2 was terminated by an intense snowmelt event lasting until 4 January 1998. Snowmelt continued until the end of the measuring period. In this phase, advection of warm humid air masses caused high ablation rates like in phase 1.

Throughout the measuring period, net radiation provided the major energy input for snowmelt (Table I); although during phase 2 clear sky conditions led to increased nocturnal radiative losses. From concurrently modelled snowmelt it can be seen that the pronounced daily cycle of the radiation balance triggered ablation (Figure 3). Regarding the mean value, sensible heat flux was a second energy source, while the latent heat flux did not result in significant ablation (Table I). The low latent heat flux is caused by averaging, since positive and negative values equalize each other over the entire measuring period. Rain heat flux contributed only 0.3% to the sum of energy balance components at AWS 1. During the different ablation phases, remarkable features can be observed. In phase 1, turbulent heat fluxes are positive, while in the second phase sensible heat flux shows the highest positive and negative amplitudes. In phase 2, the heat loss occurred due to evaporation from the snow cover. The turbulent fluxes are, therefore, characterized by a negative sign. Only on one occasion, at the beginning of January, the contribution of turbulent heat fluxes to snowmelt exceeded that of radiation balance. Phase 3 is similar to phase 1 in terms of the distribution of energy fluxes.

5.2. The influence of atmospheric circulation patterns on snowmelt

The results presented in the previous section indicated the dependence of energy balance terms on atmospheric conditions. Therefore, the calculations of local surface energy balance were combined with an analysis of concurrent synoptic-scale weather situations. The major synoptic situations were extracted
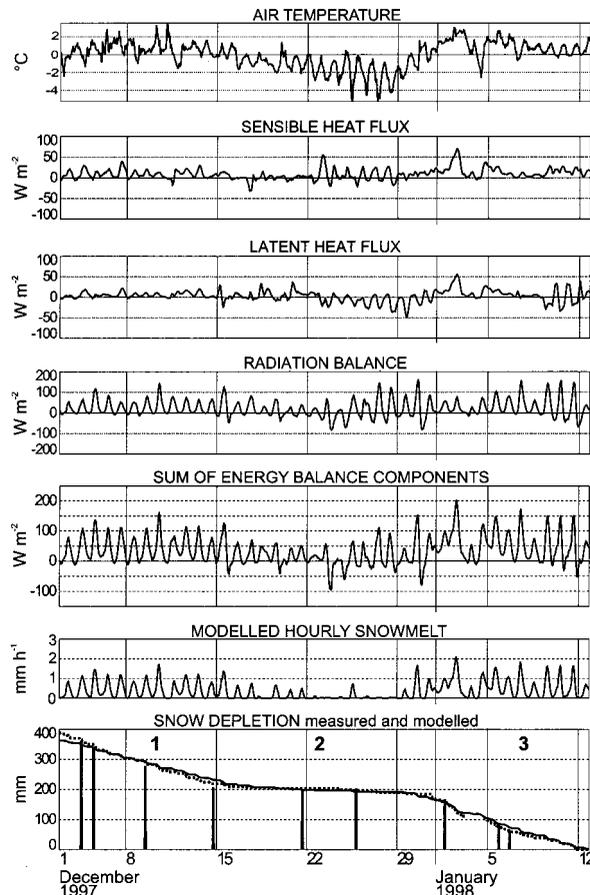
Figure 4. Energy balance components, sum of energy balance terms, modelled hourly snowmelt and snow depletion at AWS 1 for the entire measuring period. Solid line, modelled ablation; dotted line, measured ablation with snow depth sensor; bars, readings of ablation stakes

from surface pressure charts and NOAA images. An example for each synoptic situation is shown in Figure 5. Accordingly, representative radio sounding data for Bellingshausen station are plotted in Figure 6 for the four weather situations. Air temperature, sums of energy balance components and hourly melt rates are presented in Figure 7. Figure 8 shows energy balance terms averaged over time and resulting snowmelt rates for all three AWSs.

5.2.1. Advection from north to northwest (11–13 December 1997). From 9 December 1997 onwards, a synoptic scale low-pressure centre moved rapidly eastwards over the Bellingshausen Sea (Figure 5(a)). It slowed down in front of the Antarctic Peninsula and caused the advection of warm, humid air masses from the north. The frontal zone in the satellite image is clearly marked by a cloud band. In the back of this strong depression centre, a mesocyclone developed, which is not represented in the pressure chart, but is visible in the NOAA image of 11 December 1997. King and Turner (1997) report that mesocyclones often develop on the lee of synoptic-scale depressions near the frontal zone. However, the impact of that mesocyclone on surface energy fluxes was considered negligible for the purpose of this study. With the approach of the depression centre to the Antarctic Peninsula, air temperatures rose above 0°C (Figure 7(a)). In the area of the South Shetland Islands, north to northwesterly air mass transport prevailed (Figure 6(a)) and led to a predominantly overcast sky. This led to an almost balanced long-wave radiation budget and short-wave irradiance caused an intensive daily cycle of snowmelt. This could also be reproduced by the model runs as shown for AWS 1 (Figure 7(a)). The sum of energy balance terms was
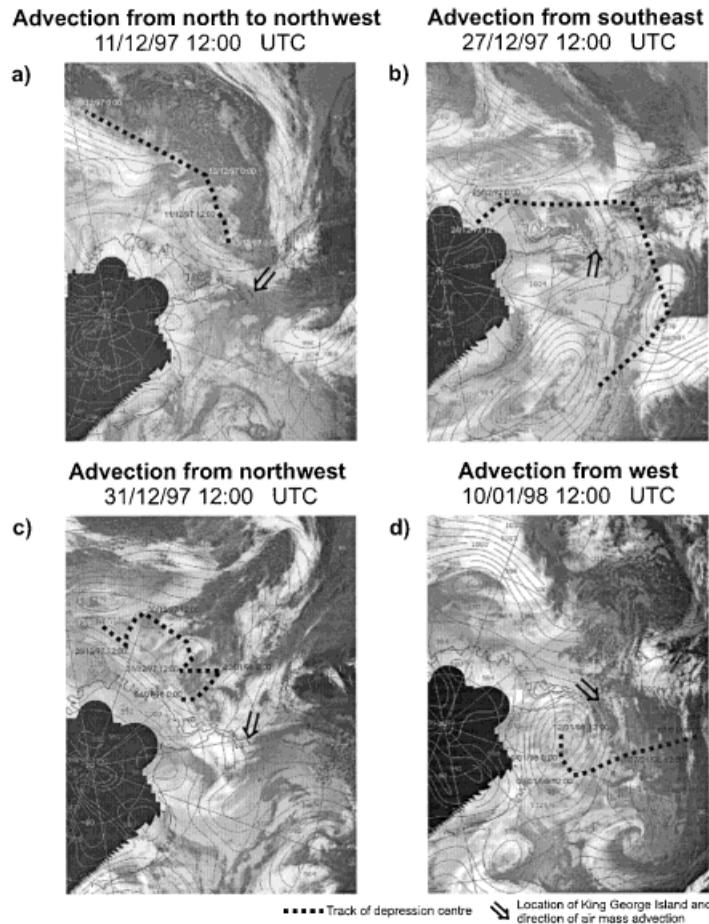
Figure 5. AVHRR IR-composites and surface pressure charts for the analysed synoptic situations. The tracks of the major depressions are marked. Reproduced by permission of Antarctic Meteorological Research Center, Space Science and Engineering Center, University of Wisconsin–Madison

positive at all three locations (Figure 8(a)), resulting in melt rates between 6 and 9 mm WE per day. This was mainly due to the positive mean radiation balance. Latent heat was found to contribute substantially to the energy balance only at the lowest site (AWS 1) and only at this site a positive sensible heat flux was observed.

   5.2.2. Advection from southeast along the Antarctic Peninsula (26–30 December 1997). This synoptic situation was characterized by a depression centre north of the Antarctic Peninsula and high pressure over the Peninsula itself. A further depression centre was located in the northeastern Weddell Sea sector. The sea level pressure chart and the radio sounding data indicate a southerly to southeasterly flow of air masses (Figures 5(b) and 6(b)). This led to the transport of cold, dry air from the central Antarctic continent along the mountain ridge of the Antarctic Peninsula towards the South Shetland Islands. Parish (1989) pointed out that air masses originating from the Weddell Sea may play a significant role in the synoptic meteorology of the South Shetland Islands. These barrier winds cannot pass the obstacle of the Antarctic Peninsula due to the strong inversion in the Weddell Sea area. Air masses are led along the mountain crest to the north where they spread and sometimes reach the South Shetland Islands. During this situation, air temperatures almost never exceed 0°C and relative humidity drops to a mean value of 75%. Such low values of relative humidity and cloud coverage persisting over several days are not very common in summer for the maritime climate of the South Shetland Islands.
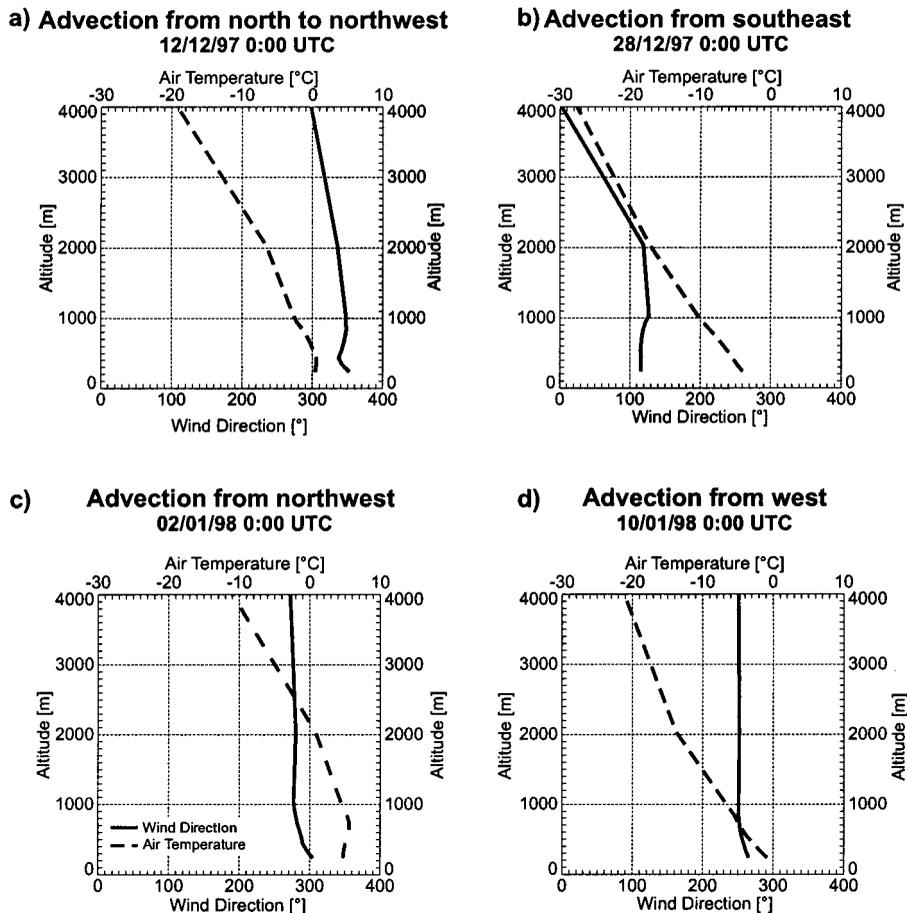
Figure 6. Representative radio sounding profiles from Bellingshausen Station during four different synoptic situations showing wind direction (solid line) and air temperature (dashed line)

It is only at the two lowermost AWSs that the mean sum of energy balance terms was slightly positive. In the highest parts of the King George Island ice cap, a mean energy loss of about $20 \ \mathrm{W \ m^{-2}}$ was calculated. This can be attributed to a significant heat loss by evaporation as a consequence of the simultaneous occurrence of air temperatures some degrees below the freezing-point, low relative humidity values and an isothermal snow cover at 0°C with a high liquid water content. Negative mean latent heat flux was observed at all AWSs, but the average net radiation was negative only at AWS 3. This synoptic situation resulted in significant daily variations of sensible heat flux at AWS site 1 (Figure 4). However, the average sensible heat flux does not reveal these daily cycles. Snowmelt was negligible during this synoptic situation. Only at the end of this period air temperatures rose above 0°C, due to an approaching depression centre in the Bellingshausen Sea (Figure 5(c)). The distribution of energy balance terms with a pronounced negative latent heat flux at the highest AWS corresponds to observations further south in the area of Marguerite Bay and Alexander Island (Jamieson and Wager, 1983; Schneider, 1999b). However, in these regions sensible heat flux provides more energy for snowmelt than net radiation.

5.2.3. Advection from northwest (31 December 1997–3 January 1998). A low pressure area in the Bellingshausen Sea and high pressure over the South American continent caused a strong meridional advection of warm, humid air masses from the northwest towards the Antarctic Peninsula. The depression centre was observed for the first time on the composite images on 28 December 1997 at about 135°W, and

a) Advection from north to northwest
11/12/97 0:00 to 14/12/97 0:00 UTC

b) Advection from southeast
26/12/97 12:00 to 30/12/97 0:00 UTC

Advection from northwest
c)   31/12/97 18:00 to 03/01/98 18:00 UTC

Advection from west
d)   07/01/98 0:00 to 12/01/98 12:00 UTC
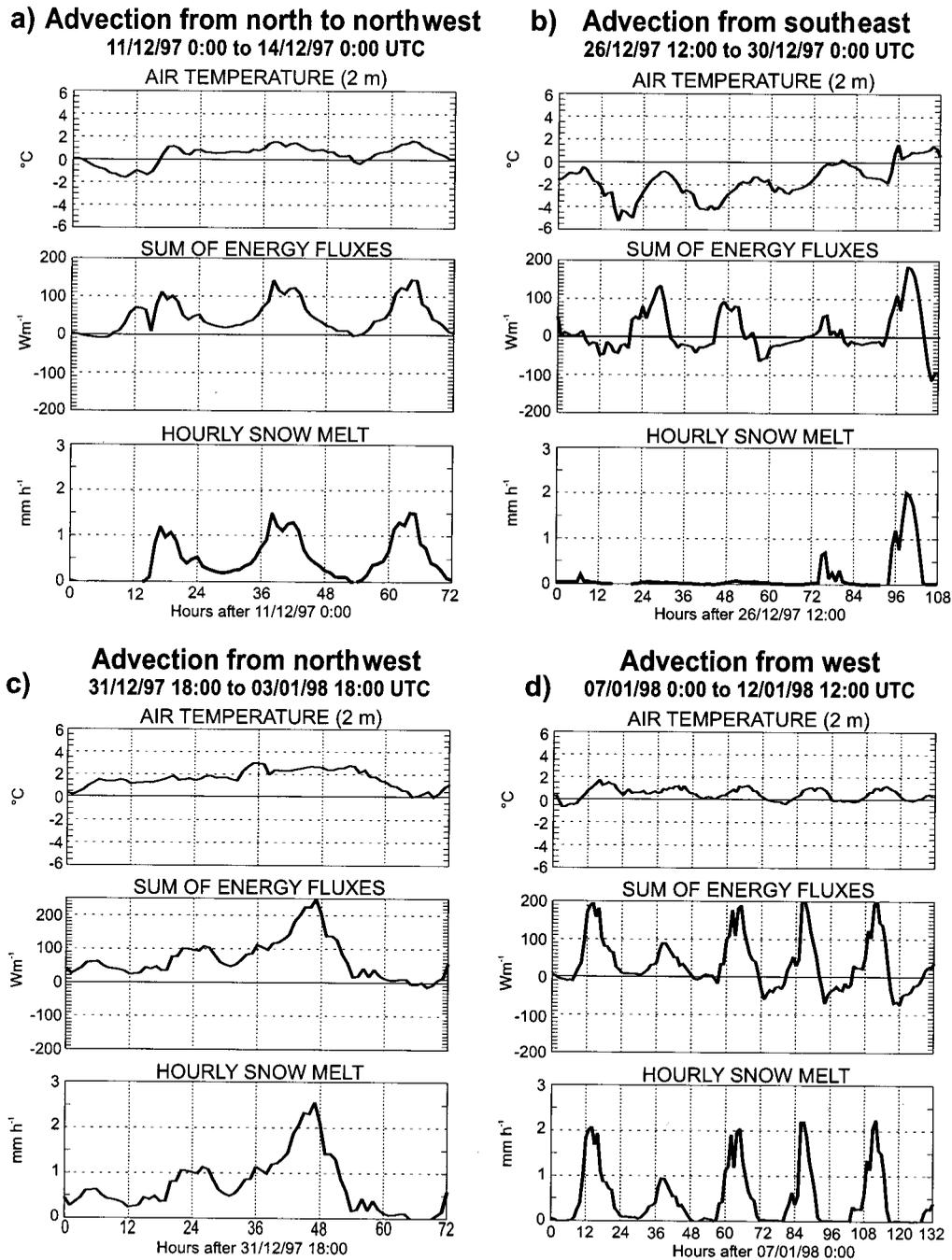
Figure 7. Air temperature, sum of energy fluxes and modelled hourly snowmelt at AWS 1 for different large-scale synoptic circulation patterns

then it moved continuously north and eastwards. During 2 January 1998, it reached its closest location to King George Island and disappeared on 4 January 1998 west of Alexander Island (Figure 5(c)). Radio sounding data show westerly winds at all altitudes up to 4000 m a.s.l. (Figure 6(c)). As a result of high wind speeds coupled with warm and humid air masses, the energy input from turbulent heat fluxes exceeded the input from net radiation. A daily cycle of snowmelt, which could have been induced by solar
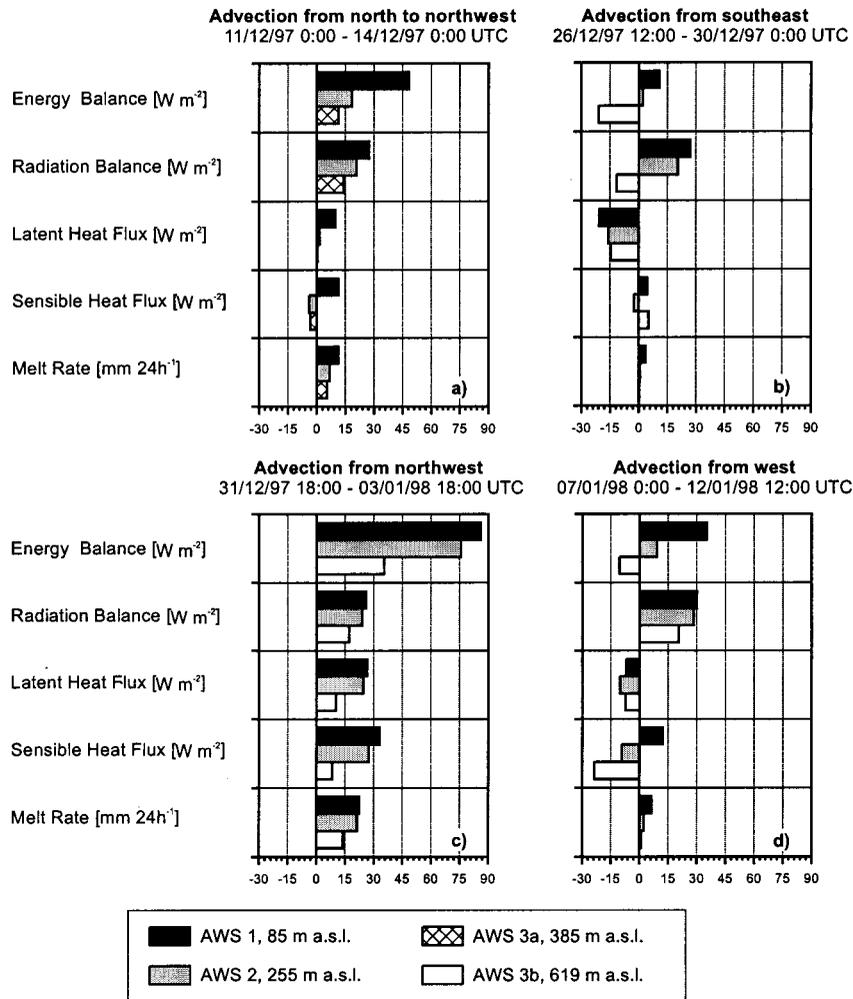
Figure 8. Mean values of energy balance components for the three AWS during different air mass advection

irradiance, was prevented by the dense cloud coverage. Therefore, the warm air masses and the positions of the pressure centres triggered snowmelt during this situation. The highest hourly melt rates of the entire field campaign were observed and modelled with up to 2.5 mm h^{-1} at AWS 1 (Figure 4). No significant altitudinal differentiation in available energy for snowmelt could be detected on this occasion. However, the contribution of net radiation to ablation was more important at higher rather than at lower altitudes (Figure 8(c)). Similarly, Hogg *et al.* (1982) found very high contributions of sensible heat fluxes to the total energy balance on South Georgia. The frequent passage of low pressure centres in that region results in high air temperatures and concurrent high wind speeds. As a consequence, high sensible heat flux is measured.

5.2.4. Advection from west (7–12 January 1998). This synoptic situation was characterized by a deep depression located in the Weddell Sea. This low originated from lower latitudes and moved into the Weddell Sea until 9 January 1998, where it persisted until the end of the measuring period (Figure 5(d)). The stable arrangement of pressure centres resulted in a westerly to southwesterly air mass transport from the Bellingshausen Sea to the region of the South Shetland Islands (Figure 6(d)). A strong daily cycle of all meteorological variables was observed (Figure 7(d)). Air temperatures almost never dropped below 0°C during night time at AWS 1 (Figure 7(d)). However, temperatures at the other AWS sites remained at or

below freezing point. This resulted in positive average sensible heat fluxes at the lowermost AWS and negative values for the higher elevations. The predominantly overcast sky (6–8 August) caused a major energy gain by net radiation at all AWS sites. Overall, heat loss occurred at all AWSs by latent heat flux. This led to moderate snowmelt rates at lower altitudes and almost no snowmelt at AWS 3.

6. DISCUSSION

The study shows that on the King George Island ice cap, the major energy input is provided by net radiation, with sensible heat flux as a secondary source. On average, latent heat flux did not contribute significantly to ablation. Similar findings were reported by Bintanja (1995) for Ecology Glacier in Admiralty Bay. The mean distribution of the energy balance components at AWS site 1 (84 m a.s.l.) and Ecology Glacier (100 m a.s.l.) coincide well. However, the absolute mean values of the present study only reach half of the energy input measured during the summer of 1991–1992 (Bintanja, 1995). This may be due to the fact that his study was conducted in a relatively warm year (1.5 K warmer than the average). Although Figure 2 shows that in January 1998 the mean monthly air temperature also exceeded the long-term monthly mean (1944–1999), December 1997 only lay within the long-term mean. The majority of the measuring period was in December 1997. Moreover, the measuring periods covered different time spans [4 weeks (Bintanja, 1995) versus 6 weeks (present paper)]. Bintanja's research period lacked a phase of low temperatures with advection from the south or southeast, where no ablation was recorded as it was in the present study. Additionally, the study site in Admiralty Bay is generally characterized by higher temperatures and less cloud. Furthermore, the occurrence of bare glacier ice at the end of the measuring period at the Ecology test site in 1991–1992 may be another reason for the higher ablation measured by Bintanja (1995).

The close correspondence between measured and modelled WE decrease indicates that the chosen model is appropriate for the conditions encountered on the ice cap. Generally, snowmelt occurred at lower elevations during almost all synoptic situations, while the highest parts of the King George ice cap were affected only by strong advection events due to meridional air mass transport. The distribution of energy balance components and melt rates differed widely depending on altitude. This corresponds to the findings by Knap *et al.* (1996), who suggested that an increase or decrease in mean air temperature would affect the lower parts of the ice cap to a greater extent.

The variation of energy balance terms and the obvious sub-division in different phases indicate that synoptic scale atmospheric circulation controls the local surface energy balance terms and therefore ablation on the King George Island ice cap. Northerly and northwesterly air flow lead to the highest ablation rates. These warm humid air masses originate from lower latitudes and are transported over the ice-free southern ocean. Kejna (1993) showed that northerly to northwesterly flow is the dominant air mass transport during the 3-year period he investigated (1986–1989). However, even the north to northwesterly advection, considerable differences in energy input and ablation occurred. This was shown by the contrasts of situation (a) and (c). While very strong pressure gradients led to meridional flow during phase (c), synoptic situation (a) was characterized by an approaching cyclone. In both situations net radiation balance reached similar values but turbulent fluxes differed greatly. Turner and Leonard (1996) also reported a quasi-stationary synoptic-scale low in the Weddell Sea, as in situation (c). In their study, the cyclone reached the highest lifetime recorded during a whole year. Kejna (1993) states that southerly flow is not very common in summer but more frequent in winter, when depressions pass by further to the north. The cold air leads to a marked decline in ablation and to the refreezing of liquid water within the snow pack at higher altitudes on the ice cap. Carleton (1992) reports that southerly flow from the Weddell Sea is more frequent in El Niño years and causes a marked delay of sea ice disappearance near the South Orkney Islands as was the case in 1997–1998. One may speculate now that this unusually long period of southerly and easterly flow is a consequence of these anomalies in the Southern Hemisphere circulation, but more research is needed to collect further conclusive evidence.

7. CONCLUSIONS

The data from a field campaign during the austral summer 1997–1998 provided information on surface energy balance components during different synoptic situations. A strong dependence of calculated surface energy fluxes and ablation rates on large-scale atmospheric circulation patterns could be demonstrated. This is especially interesting, since indications for changes in the atmospheric circulation in the region of the Antarctic Peninsula are given by several authors. Turner *et al.* (1997) analysed the precipitation records of Faraday and Rothera stations and found that the precipitation pattern changed during the last decades towards more rain and generally more precipitation events. They explained this through more frequent air mass advection from the north. Similarly, King and Harangozo (1998) attribute the rising air temperatures along the Antarctic Peninsula to an increase in air mass transport from a northerly direction. The highest significance for this type of climatic changes can be expected during winter and for areas further south than the South Shetland Islands. This is supported by results of Fox and Cooper (1998) for the Marguerite Bay area. They found a considerable increase in positive degree days since the 1960s and a decrease in the number of snowfall events. However, Rachlewicz (1997) already showed, that winter warm-air advection can result in extraordinarily high snowmelt on King George Island. Therefore, the ice cap of King George Island seems to be highly sensitive to climatic changes since summer ablation and winter accumulation will be affected by a change in the large-scale circulation pattern to more frequent northerly flow.

The high positive temperature trend along the Antarctic Peninsula was derived from monthly or yearly mean values. However, the current results indicate that sensitivity studies based on the addition of 1 K to air temperature of a short data set are very limited.

A change in the frequency of certain synoptic weather situations does not only result in air temperature increase, but in the modification of other meteorological variables as well. A higher frequency of northerly advection will increase the ablation days, whereas in terms of a sensitivity study a general increase of 1 K affects only periods where the sum of energy balance is already positive or nearly in balance. Consequently, the approach of a general 1 K addition results in a different process modelling than changing the frequency of typical synoptic situations. However, more accurate analyses of synoptic weather patterns and their frequencies over several years are required to base sensitivity studies on this approach.

REFERENCES

Anderson PS. 1994. A method for rescaling humidity sensors at temperatures well below freezing. *Journal of Atmospheric and Oceanic Technology* **11**: 1388–1391.
Bintanja R. 1995. The local surface energy balance of Ecology Glacier, King George Island. *Antarctic Science* **7**: 315–325.
Blackadar AK. 1997. *Turbulence and Diffusion in the Atmosphere*. Springer: Berlin.
Braithwaite RJ. 1995. Aerodynamical stability and turbulent sensible-heat flux over a melting ice surface, the Greenland ice sheet. *Journal of Glaciology* **41**: 562–571.
Braun L. 1985. Simulation of snowmelt-runoff in lowland and lower alpine regions of Switzerland. *Züricher Geographische Schriften* **21**: 166.
Braun M, Schneider C. 2000. Characteristics of summertime energy balance on the west coast of the Antarctic Peninsula. *Annals of Glaciology* **31** (in press).

Braun M, Rau F, Saurer H, Goßmann H. 2000. The development of radar glacier zones on the King George Island ice cap (Antarctica) during the austral summer 1996–1997 as observed in ERS-2 SAR data. *Annals of Glaciology* **31** (in press).

Carleton AM. 1992. Synoptic interactions between Antarctica and lower latitudes. *Australian Meteorological Magazine* **40**: 129–147.

Fox AJ, Cooper APR. 1998. Climate change indicators from archival aerial photography of the Antarctic Peninsula. *Annals of Glaciology* **27**: 636–642.

Harangozo SA, Colwell SR, King JC. 1997. An analysis of a 34-year air temperature record from Fossil Bluff (71°S, 68°W), Antarctica. *Antarctic Science* **9**: 355–363.

Heinemann G. 1995. Polare Mesozyklonen. *Bonner Meteorologische Abhandlungen* **45**: 157.

Hock R. 1998. Modelling glacier melt and discharge. *Züricher Geographische Schriften* **70**: 126.

Hogg IGG, Paren JG, Timmis RJ. 1982. Summer heat and ice balances on Hodges Glacier, South Georgia, Falkland Islands Dependencies. *Journal of Glaciology* **28**: 221–238.

Jamieson AW, Wager AC. 1983. Ice, water and energy balances of Spartan Glacier, Alexander Island. *British Antarctic Survey Bulletin* **52**: 155–186.

Jones DA, Simmonds I. 1993. A climatology of Southern Hemisphere extratropical cyclones. *Climate Dynamics* **9**: 131–145.

Kejna M. 1993. Types of atmospheric circulation in the region of H. Arctowski station (South Shetland Islands) in years 1986–1989. In *XX Polar Symposium: Main Impact on Polar Environment, Lublin, Poland*, Replelewska-Pekalowa J, Kazimierz P (eds); 369–375.

King JC. 1994. Recent climate variability in the vicinity of the Antarctic Peninsula. *International Journal of Climatology* **14**: 357–369.

King JC, Harangozo SA. 1998. Climate change in the western Antarctic Peninsula since 1945: observations and possible causes. *Annals of Glaciology* **27**: 571–575.

King JC, Turner J. 1997. *Antarctic Meteorology and Climatology*. Cambridge Atmospheric and Space Science Series, Cambridge University Press: Cambridge; 409.

Knap WH, Oerlemans J, Cadée M. 1996. Climate sensitivity of the ice cap of King George Island, South Shetland Islands, Antarctica. *Annals of Glaciology* **23**: 154–159.

Kuhn M. 1979. On the computation of heat transfer coefficients from energy-balance gradients on a glacier. *Journal of Glaciology* **22**: 263–272.

Martianov V, Rakusa-Suszczewski S. 1990. Ten years of climate observations at the Arctowski and Bellingshausen station (King George Island, South Shetland Islands, Antarctica). In *Global Change Regional Research Centres: Scientific Problems and Concept Developments*. Warsaw-Jablonna, IGBP IASA UNESCO PAS Seminar, Birkenmajer A (ed.). Institute of Geography and Spatial Organization: Warsaw, Poland; 80–87.

Moore RD. 1983. On the use of bulk aerodynamic formulae over melting snow. *Nordic Hydrology* **14**: 193–206.

Morris EM. 1989. Turbulent transfer over snow and ice. *Journal of Hydrology* **105**: 205–223.

Morris EM, Harding RJ. 1991. Parametrization of turbulent transfer between glaciers and the atmosphere. *International Association of Hydrological Sciences (IHAS) Publication* **208**: 543–549.

Neal SM, Fitzharris BB. 1997. Energy balance and synoptic climatology of a melting snowpack in the southern alps, New Zealand. *International Journal of Climatology* **17**: 1595–1609.

Oke TR. 1970. Turbulent transport near the ground in stable conditions. *Journal of Applied Meteorology* **9**: 778–786.

Parish TR. 1989. The influence of the Antarctic Peninsula on the wind field over the Western Weddell Sea. *Journal of Geophysical Research* **88**: 2684–2692.

Park B-K, Chang S-K, Yoon HI, Chung H. 1998. Recent retreat of ice cliffs, King George Island, South Shetland Islands, Antarctic Peninsula. *Annals of Glaciology* **27**: 633–635.

Rachlewicz G. 1997. Mid-winter thawing in the vicinity of Arctowski Station, King George Island. *Polish Polar Research* **18**: 15–24.

Reynolds JM. 1981. The distribution of mean annual temperatures in the Antarctic Peninsula. *British Antarctic Survey Bulletin* **54**: 123–131.

Schneider C. 1999a. Energy balance estimates during the summer season of glaciers of the Antarctic Peninsula. *Global and Planetary Change* **22**: 117–130.

Schneider C. 1999b. Zur raumzeitlichen Differenzierung der Energiebilanz auf zwei Gletschern in der Marguerite Bay-Aspekte des Klimas und des Klimawandels am Rande der Antarktis. *Freiburger Geographische Hefte* **56**: 245.

Schwerdtfeger W. 1984. Weather and climate of the Antarctic. *Developments in Atmospheric Science* **15**: 261.

Simões JC, Bremer UF, Aquino FE, Ferron FE. 1999. Morphology and variations of glacial drainage basins in the King George Island ice field, Antarctica. *Annals of Glaciology* **29**: 220–224.

Skvarca P, Rack W, Rott H, Ibarzábal y Donángelo T. 1998. Evidence of recent climatic warming on the eastern Antarctic Peninsula. *Annals of Glaciology* **27**: 628–932.

Smith RC, Stammerjohn SE, Baker KS. 1996. Surface air temperature variations in the western Antarctic Peninsula region. *Antarctic Research Series* **70**: 105–121.

Stark P. 1994. Climatic warming in the central Antarctic Peninsula area. *Weather* **49**: 215–220.

Turner J, Leonard S. 1996. Synoptic scale weather systems around the Antarctic Peninsula from satellite imagery and model fields. 8th Conference on Satellite Meteorology and Oceanography, 28 January–2 February 1996, Atlanta, GA.

Turner J, Colwell SR, Harangozo S. 1997. Variability of precipitation over the coastal western Antarctic Peninsula from synoptic observations. *Journal of Geophysical Research* **102**: 13999–14007.

Turner J, Marshall GJ, Lachlan-Cope TA. 1998. Analysis of synoptic scale low pressure systems within the Antarctic Peninsula sector of the circumpolar trough. *International Journal of Climatology* **18**: 253–280.

Wen J, Kang Y, Xie Z, Han J, Lluberas A. 1994. Climate, mass balance and glacial changes on small dome of Collins ice cap, King George Island, Antarctica. *Antarctic Research* **5**: 52–61.

Wen J, Kang J, Han J, Xie Z, Liu L, Wang D. 1998. Glaciological studies on King George Island ice cap, South Shetland Islands, Antarctica. *Annals of Glaciology* **27**: 105–109.

Wunderle S. 1996. Die Schneedeckendynamik der Antarktischen Halbinsel und ihre Erfassung mit aktiven und passiven Fernerkundungsverfahren. *Freiburger Geographische Hefte* **48**: 172.